

Preparation of a soft and interconnected macroporous hydroxypropyl cellulose methacrylate scaffold for adipose tissue engineering

Cite this: *J. Mater. Chem. B*, 2013, **1**, 3107

Siew Pei Hoo,^{abc} Qiu Li Loh,^d Zhilian Yue,^e Jing Fu,^f Timothy T. Y. Tan,^g Cleo Choong^{*d} and Peggy P. Y. Chan^{*bc}

This study describes the preparation and characterization of a biodegradable 3D hydrogel constructed from hydroxypropyl cellulose (HPC), modified with bifunctional methacrylic anhydride (MA) to form hydroxypropyl cellulose methacrylate (HPC-MA), for adipose tissue engineering applications. The hydrogels were prepared from three different concentrations (10 wt%, 15 wt% and 20 wt%) of HPC-MA with 0.35 degree of substitution. HPC-MA hydrogel scaffolds with open biphasic features were prepared by exploiting the thermal responsive phase behavior of HPC and temperature mediated phase separation of HPC-MA. The resulting scaffolds exhibited pore sizes ranging from 30 to 300 μm and an interconnected porosity of $\sim 90\%$. The swelling ratio (SR) and storage modulus of HPC-MA scaffolds were in the range of 12.94 to 35.83 and 0.75 to 4.28 kPa, respectively. The swelling ratio and storage modulus suggested that the scaffold exhibits high water retention, allowing medium exchange during cell culturing and that it is suitable for adipose tissue regeneration. The HPC-MA scaffolds were found to be biocompatible to human adipose-derived stem cells (ASCs). ASCs were successfully differentiated into the adipocytes inside the scaffolds, and therefore demonstrated the potential application of these HPC-MA scaffolds for adipose tissue engineering.

Received 21st November 2012

Accepted 30th April 2013

DOI: 10.1039/c3tb00446e

www.rsc.org/MaterialsB

Introduction

Currently, there is a need for transplantable and functional adipose tissue to restore lost or damaged tissue due to post-traumatic loss, lipoatrophy, tumor removal or congenital defects.^{1–3} A scaffold-based tissue engineering approach is a promising alternative to current autologous fat grafts as it addresses the issue of donor site morbidity as well as other complications associated with fat graft transfers including fat necrosis and volume reduction over time.⁴ In general, an ideal scaffold for adipose tissue application should: (1) be constructed from materials with controlled biodegradability or bioresorbability so that new adipose tissues will eventually

replace the scaffold, (2) possess an extensive network of inter-connecting pores to promote nutrient and waste exchange, (3) provide appropriate surface chemistry to facilitate cellular attachment, differentiation and proliferation, (4) be easily fabricated into a variety of shapes and sizes, (5) mimic the soft and elastic texture of native tissues, and (6) provide appropriate mechanical strength that can withstand post-implantation forces exerted on the tissue.^{5–7} The mechanical properties of the scaffold are of particular importance as mechanical stimulus has been shown to regulate the differentiation response of seeded stem cells.⁸ Ideally, the scaffolding material should mimic the property of the tissue it is replacing, and in the case of adipose tissue, a Young moduli range of 3–4 kPa has been reported.^{9,10}

Cell-based tissue engineering using scaffolds offers great promise for repair of adipose tissue. Human adipose-derived stem cells (ASCs) are multipotent mesenchymal stem cells derived from the stromal vascular fraction of adipose tissue, and are available abundantly as they can be isolated from adipose tissue by liposuction or abdominoplasty.^{11,12} ASCs are capable of differentiating into a variety of mesenchymal lineages including mature adipocytes.^{9,13,14} ASCs have also been shown to secrete factors that trigger host stem cell migration to the implantation site, thus contributing to tissue regeneration. Increasing evidence suggested that increases in adipose tissue are associated with increases in microcirculation.² ASCs have

^aDepartment of Chemical Engineering, Monash University, Australia. E-mail: siew.hoo@monash.edu

^bMicroNanophysics Research Laboratory, School of Applied Science, RMIT University, Australia. E-mail: peggy.chan@rmit.edu.au; Tel: +613 9925 2660

^cMelbourne Centre for Nanofabrication, Clayton, Australia

^dSchool of Materials Science and Engineering, Nanyang Technological University, Singapore. E-mail: cleochoong@ntu.edu.sg; Fax: +65 6790 908; Tel: +65 6513 8166

^eARC Centre of Excellence for Electromaterials Science, Intelligent Polymer Research Institute, AIIIM facility University of Wollongong, Australia. E-mail: zyue@uow.edu.au

^fDepartment of Mechanical and Aerospace Engineering, Monash University, Australia. E-mail: jing.fu@monash.edu

^gSchool of Chemical & Biomedical Engineering, Nanyang Technological University, Singapore. E-mail: TTYTan@ntu.edu.sg

also been shown to modulate immune response and have the potential to avoid tissue rejection.⁹ ASCs are therefore an attractive cell source for adipose tissue engineering and regenerative therapeutic applications.

The use of a 3-dimensional (3D) scaffold as an ASCs culturing system is considered to be advantageous compared to 2-dimensional (2D) monolayer culture, since 3D systems can closely mimic the microenvironment that cells experience *in vivo*.¹⁵ Girandon *et al.* have demonstrated that the ASC cultured in a 3D scaffold expressed higher levels of specific adipogenic markers compared to 2D culture.¹⁶ A literature review by Flynn and Woodhouse¹⁷ has summarized the results from studies that investigate the use of a range of synthetic and naturally derived scaffolds for adipose tissue engineering. Although a number of scaffolds have shown to facilitate adipose tissue regeneration, new biomaterials are still required to provide multifunctional platforms that incorporate biochemical and physiochemical properties that can be beneficial to adipose tissue engineering.

Scaffold pore sizes, porosity and pore interconnectivity are critical parameters that influence cell binding, migration, intracellular signalling, vascularization, ECM production, cell phenotype, nutrient transport, gas diffusion, and metabolic waste removal, thus determining scaffold performance. The pore size of the 3D scaffold must be large enough to accommodate the increase in cell number and the increase in volume associated with lipid formation⁵ and for cells to migrate through the pores, but the pore size should also be small enough to retain a critical total surface area for appropriate cell binding.^{18,19} There has not been extensive research on the optimum pore size for human adipose-derived stem cells. However, in general, the accepted optimum pore size of tissue scaffolds for the majority of mammalian cells such as liver tissue regeneration, fibroblast ingrowth and bladder smooth muscle cell attachment and ingrowth should be within the range of 38 to 500 μm , and the optimum porosity should be above 90%.^{18–23} A variety of techniques have been developed to fabricate porous structures including solvent casting, gas forming, solvent-casting and porogen leaching, solvent induced phase separation, electrospinning, emulsion freeze drying, fiber bonding, or a mixture of these techniques. Although these techniques can produce highly porous scaffolds, these methods have a limited control over scaffold architecture, pore interconnectivity, poor strength and in some instances require the use of toxic solvent.^{20–22} For example, the solvent-casting and porogen leaching method produces porous structure with controllable pore size and porosity, however the resulting scaffolds often exhibit porous structure with closed pore walls, thus impeding nutrient transport and cell infiltration within the scaffold.²⁴

There is a growing awareness of developing biomaterials using renewable resources such as cellulosic materials.^{25,26} Hydroxypropyl cellulose (HPC) is a commercial derivative of cellulose and Food and Drug Administration (FDA)-approved agent for drug delivery applications. HPC is available abundantly at low cost, soluble in water as well as in a variety of organic solvents, commercially available in a range of molecular weights, making it an attractive biomaterial. More importantly,

HPC exhibits phase transition from isotropic aqueous solution to a meta-stable biphasic system above its lower critical solution temperature.^{26,27} In a previous study,²⁶ hydroxypropyl cellulose (HPC) was modified with allyl isocyanate containing urethane group and fabricated into a 3D interconnected porous scaffold by immobilizing biphasic HPC *via* gamma-ray irradiated crosslinking. This method produced biocompatible scaffolds with interconnected macroporous structure with a porosity of approximately 90%. Despite the advantages of allyl isocyanate modified HPC, it is not biodegradable due to the lack of cellulose hydrolyses *in vivo*. In addition, polymers with repeating unit that contains urethane moiety are generally regarded to have limited biodegradability. For example, polyurethanes are typically used as non-biodegradable coatings. Synthesis of biodegradable polyurethane requires the polyurethane to be produced from diisocyanate precursor such as lysine-diisocyanate that releases nontoxic degradation products such as lysine.²⁸

Herein, we prepare biodegradable and macroporous scaffold structures taking advantages of the temperature responsive property of HPC. HPC was first modified with a bifunctional methacrylic anhydride (MA). The resulting conjugate contains a photo-crosslinkable and hydrolytically degradable methacrylate pendant group. The modified HPC conjugates, namely HPC-MA, were polymerized at its colloidal state induced by temperature mediated phase separation, thereby immobilizing the biphasic feature of HPC. The phase separation was induced in aqueous solvent simply by warming an aqueous solution containing HPC-MA to above 40 °C, and avoids the use of organic solvent and thus the problem associated with harmful organic solvent residues. The physiochemical properties such as swelling ratio, porosity, mechanical properties and interior morphologies of these HPC-MA scaffolds were evaluated. Cytotoxicity studies using human adipose-derived stem cells (ASCs) were carried out to examine the biocompatibility of the scaffold. The current novel HPC-MA scaffold was then investigated as a support for the proliferation and adipogenesis of ASCs.

Experimental

Synthesis scheme and ¹H nuclear magnetic resonance (NMR)

Hydroxypropyl cellulose (HPC, M_n 10 000 g mol⁻¹, Sigma-Aldrich) was dehydrated by azeotropic distillation at 50 °C in toluene to remove the moisture before use. The HPC hydrogel precursor, namely the HPC-MA conjugate, was prepared by modifying cellulose with methacrylic anhydride (MA). Briefly, 4.0 g of dehydrated HPC was dissolved in 150 mL of chloroform followed by 4.17 mmol of methacrylic anhydride (MA). 4.17 mmol of *N,N*-dicyclohexylcarbodiimide (DCC) was first dissolved in 3 mL of chloroform before adding dropwise in the HPC chloroform mixture. The solution was stirred for 48 h in the presence of 0.4 g of 4-dimethylaminopyridine (DMAP) as catalyst. The product was concentrated and precipitated into diethyl ether. Further purification was carried out by repeating dissolution in chloroform and precipitation into diethyl ether. Finally, the product was dissolved in water, filtered, and dialyzed against deionised water for 72 h before lyophilisation in a

freeze dryer (HETO PowerDry PL6000, Thermo Scientific). The ^1H NMR spectra of the lyophilised HPC-MA sample were obtained in deuterated chloroform (CDCl_3) using a NMR operating at 300 MHz (Bruker, ACF 300).

Preparation of HPC scaffolds and turbidity

The turbidity of the HPC-MA conjugate was measured to determine its lower critical solution temperature. A 10% w/v HPC-MA aqueous solution was selected as an indication of the LCST. In brief, the lyophilised HPC-MA was dissolved in deionised water. The transmittance of the sample was monitored as a function of temperature at a fixed wavelength of 500 nm, using a UV/Vis spectrophotometer (Agilent Technologies Cary 60 UV-VIS, Australia) with the sample cell thermostatted by a temperature controller with a circulating water bath. The transmittance was measured four times and the average transmittance values of the measurement were reported.

Lyophilised HPC-MA conjugate was dissolved in deionised water (10%, 15% and 20% w/v respectively), followed by adding 3–5% final concentration of 2-hydroxy-1-[4-(2-hydroxyethoxy)-phenyl]-2-methyl-1-propanone, known as Irgacure 2959 (Sigma-Aldrich), as a photoinitiator. The solution was placed in a water bath at 45 °C for 10 minutes to induce phase separation. The emulsion solution was then crosslinked in a ultra-violet ray (UV) crosslinker (Honle UV Technology, UV-F 400) for approximately 6 minutes. The crosslinked gels were then washed with deionised water to remove any un-crosslinked HPC-MA conjugate and photoinitiator before lyophilisation. HPC scaffolds, after reaching their maximum swollen state in water at room temperature, were frozen at –20 °C in a freezer and lyophilised under vacuum for 48 h until all water was sublimed. The scaffolds prepared from 10%, 15%, and 20% (w/v) of HPC-MA were denoted as HPC-MA-10%, HPC-MA-15%, and HPC-MA-20%, respectively.

Swelling ratio and mechanical properties

The swelling ratio of the scaffold was measured using a conventional gravimetric method. The lyophilised HPC scaffolds with different polymer concentrations were submerged in water at room temperature for 48 h. The weight of the swollen sample was obtained after wiping off excess water on the surface with a moist filter paper and the dry weight of the sample was measured after drying the sample under vacuum at 25 °C for 48 h. The swelling ratio, SR, of the scaffold was calculated according to eqn (1) below,

$$\text{SR} = \frac{W_h - W_d}{W_d} \quad (1)$$

where W_h is the weight of the scaffold in the swollen equilibrium and W_d is the weight of the dried scaffold. Each sample was measured three times from the four replicate specimens and the average value of the measurement was taken.

Compression test was carried out to determine the mechanical properties of hydrated scaffolds with different polymer concentrations using a dynamic mechanical analyzer (TA Instruments, Q800) at a frequency of 1 Hz and a preload of

0.01 N. The testing was performed under atmospheric condition and at 298 K. The compression testing was performed in quadruplicate.

Interior morphology, porosity and mercury intrusion porosimetry

The lyophilised samples of different polymer concentrations were fractured carefully and their interior morphology was studied by using a scanning electron microscope (SEM) (FEI Quanta 200 ESEM with an EDAX Si(Li) X-ray detector and a Gatan Alto Cyro stage) after the samples have been coated with gold and palladium for 30 s.

The interconnecting pores in the HPC-MA scaffold were assessed by performing Focused Ion Beam (FIB) milling to probe the scaffold interiors, similar to the approach detailed in Al-Abboodi *et al.*²⁹ All FIB/SEM experiments were based on a Helios Nanolab 600 (FEI company), and a highly focused ion beam (30 kV, Ga^+) of large current (21 nA) was used to ablate an area of approximately $500 \times 500 \mu\text{m}$ on the scaffolds. The ablation process was continuously monitored by SEM, until an ablation depth close to 50 μm has been achieved.

The porosities of the scaffolds were determined using the solvent replacement method. In brief, lyophilised samples were first submerged in absolute ethanol for 24 h, and weighed after excess ethanol on the surface was blotted. Each sample was measured three times from the four replicate specimens and the average value of the measurement was taken. The porosity of the scaffold was calculated according to eqn (2) below,

$$\text{Porosity} = \frac{M_h - M_d}{\rho V_t} \times 100\% \quad (2)$$

where M_d and M_h are the weight of the scaffold before and after the immersion in absolute ethanol respectively. ρ is the density of absolute ethanol and V_t is the total volume of the scaffold.

The pore size distribution was determined using a mercury intrusion porosimetry (MIP) method. The interconnected pore size distribution of the lyophilised scaffold was measured out by carefully fracturing into the desired size and weight before testing using a mercury porosimeter (Autopore III, Micromeritics Co.).

Degradation study

Degradation study was carried out using the HPC-MA hydrogel disks at different concentrations with dimensions of 1 cm diameter and 1 mm thickness. It is known that the polymer containing ester linkage undergoes hydrolysis in the presence of phosphate buffered saline solution (PBS),^{30,31} therefore, the degradation study of the HPC-MA hydrogel containing a hydrolytically degradable methacrylate pendant group (ester linkage) was carried out in PBS solution. The hydrogel disks were incubated in 5 mL of PBS (pH 7.4) at 37 °C and shaken at 150 rpm for 40 days in a shaking incubator. The PBS solution was replaced every 5 days throughout the study. At pre-determined time points (5 days), the samples were rinsed with deionised water, dried in a vacuum oven for 48 h at 40 °C. Their

weight loss was then recorded. These experiments were performed with four replicates.

Surface functionalization of the scaffold and cell culture of adipose-derived stem cells (ASCs)

Lyophilised HPC-MA-10 wt% scaffolds were decontaminated by soaking in 70% ethanol overnight followed by washing with sterile phosphate buffered saline (PBS) before surface functionalisation. Sterilized scaffolds were activated in 40 nM 1,1'-carbonyldiimidazole (CDI) in acetone at room temperature for 3 h. The activated scaffolds were then washed in acetone for 3 to 4 times to remove any unreacted traces of CDI. After washing, the activated scaffolds were treated with gelatin (1.16 mg mL^{-1}) in a sodium bicarbonate (NaHCO_3) buffer (50 mM, pH 9) at room temperature for 24 h. The conjugated scaffolds were washed twice with sterile PBS before lyophilisation.

StemPro® human derived stem cells (P3) were cultured in a complete medium comprising of Dulbecco's Modified Eagle Medium Nutrient Mixture F-12 (DMEM-F12), supplemented with 10% fetal bovine serum, 1% non-essential amino acid, 1% L-glutamine and 1% P/S solution at 37 °C in a humidified atmosphere of 5% CO_2 (all chemicals and cells were obtained from Life Technologies). The medium was changed every 48 h.

ASCs were trypsinised using 0.25% trypsin upon confluence and seeded onto the sterilized scaffolds. The scaffolds were decontaminated by immersion in ethanol for 24 h with subsequent change of ethanol every 4 h, followed by rinsing in phosphate buffered saline (Life Technologies) and final immersion in DMEM-F12 solution. The scaffolds were subsequently dried and 30 μL of cell suspension was added dropwise at a density of 34 000 cells per cm^3 to the scaffold. After 4 hours, a complete medium was added for subsequent culture. Adipogenesis of ASCs in the scaffolds was also carried out by supplementing the cells with adipogenic medium. The medium was changed every 3 days.

Morphology and proliferation of ASCs in scaffolds

The surface and cross-sectional morphologies of the scaffolds as well as ASCs morphology after 14 days of *in vitro* culture were analysed using scanning electron microscopy (SEM) (JEOL JSM-5410, Japan). The cell-scaffolds were first fixed in 2.5% glutaraldehyde for 2 h, followed by a series of dehydration in graded ethanol (50%, 70%, 80%, 90%) with 15 min incubation at each interval, and final immersion in 100% ethanol for 30 min. Hexamethyldisilazane was subsequently added to the scaffolds and left to incubate for 1 h before removal and left for overnight drying at room temperature. The scaffolds were subsequently frozen in liquid nitrogen before being freeze-fractured into several sections and coated with gold prior to imaging. An acceleration voltage of 5 kV was used and images were obtained at different magnifications.

The capability of ASCs to proliferate in the scaffolds was analyzed using the alamarBlue® assay on days 2, 4 and 7. At each time point, 200 μL of 10% alamarBlue® dye (diluted with a complete medium) was added to each scaffold and incubated for 4 h at 37 °C in a humidified atmosphere of 5% CO_2 . Fluorescence analysis using an excitation wavelength of 570 nm and

an emission wavelength of 585 nm was carried out with a Thermo Scientific Varioskan Flash Multimode Reader. The number of cells corresponding to the particular relative fluorescence unit (RFU) was subsequently obtained from the standard curve (plot of RFU vs. known cell numbers).

Adipogenic characterization of ASCs and gene expression (RT-PCR)

Day 2, 4, 7 and 14 cell cultured scaffolds were fixed in 4% paraformaldehyde (Sigma-Aldrich) for 30 min and cryosectioned into thin sections of 30 μm each. 200 μL of 60% Oil Red O stain (Sigma-Aldrich) was added onto the sections and left to incubate for 5 min before imaging under the light microscope (Carl Zeiss Primo Vert).

Adipogenesis of ASCs in the scaffolds was also determined by quantifying the amount of adiponectin and leptin released over a period of 14 days using Human Adiponectin and Leptin ELISA assay kits (Raybiotech). All media were collected at each medium change and frozen at -80 °C before testing. The assays were performed according to manufacturer's instructions. Fluorescence analysis was carried out at 450 nm using the Gemini EM Microplate Reader.

Adipogenic differentiation of ASCs after 14 days of culture in the adipogenic medium was also confirmed by RT-PCR analysis. Undifferentiated ASCs cultured in a complete DMEM-F12 medium was also used as a control. Scaffolds were homogenized in trizol reagent and the RNA was extracted using the Total RNA kit I (Omega Bio-Tek). The cDNA was synthesized from the total RNA using the iScript™ cDNA Synthesis Kit (Biorad). The cDNA was used as the template in a 20 μL reaction mixture containing a specific primer pair of each cDNA according to the sequences with SYBR® Green Supermix (Biorad) (Table 1) for PCR analysis. The mRNA levels were normalized to those of GAPDH, and changes in gene expression were calculated as fold changes (the $\Delta\Delta\text{Ct}$ method).

Statistical analysis

All experiments were performed with at least three replicates. Results were reported as average value \pm standard deviation. One-way analysis of variance (ANOVA) was used to compare multiple groups of data statically; *p* values lower than 0.05 were considered statistically significant.

Table 1 PCR primers

Gene	5' to 3' sequence (sense)	5' to 3' sequence (antisense)
GAPDH	CCCCTTCATTG ACCTCAACTACA	TTGCTGATGAT CTTGAGGCTGT
PPARG	CTCCTATTGA CCCAGAAAGC	GTAGAGCTGAG TCTTCTCAG
LPL	ATGGAGAGCAA AGCCCTGCTC	GTTAGGTCCAGC TGGATCGAG
Leptin	GTGCC-TATCCAG AAAGTCCAG	TCAGCATTTCAG GGCTAACA TC
Adiponectin	CATGACCAGGAA ACCACGACT	TGAATGCTG AGCGGTAT

Results and discussion

HPC-MA characterization and hydrogel preparation

HPC-MA conjugate was synthesized by modifying HPC with MA as depicted in Fig. 1a. The degree of substitution (DS) was ~ 0.35 as calculated by $^1\text{H NMR}$ in CDCl_3 . $^1\text{H NMR}$ (CDCl_3 , δ ppm): 0.5–1.5 ($-\text{CH}_3-\text{CH}-$), 1.8–2.0 ($\text{CH}_3-\text{C}=\text{CH}_2$), 5.5–6.2 ($-\text{C}=\text{CH}_2$), 2.5–5.3 (other protons) (Fig. 1b). The degree of modification is defined as the substitution degree of available $-\text{OH}$ groups on the HPC chain. Fig. 1c demonstrated that the HPC-MA retains the phase behaviour characteristic of HPC. The LCST of HPC-MA was determined to be approximately 40 to 41 $^\circ\text{C}$, after which the transmittance decreases drastically with increasing temperature until reaching a plateau at ~ 45 $^\circ\text{C}$. HPC-MA with 0.35 DS was selected as an example for scaffold preparation. The porous HPC-MA hydrogel was produced using simple procedures without the use of porogens as illustrated in Fig. 1d. HPC-MA conjugates with 0.35 DS are water-soluble and formed single-phase solution when dissolved in aqueous solution (Fig. 1d Step 1). HPC-MA exhibited low critical solution temperature (LCST) transition at around 40 $^\circ\text{C}$. Upon heating the solution above its LCST, HPC-MA solution underwent phase transition from isotropic solution to colloidal solution (Fig. 1d Step 2). Fixation of the colloidal structure of HPC-MA was achieved by polymerizing the HPC-MA conjugate and produced an opaque hydrogel (Fig. 1d Step 3). UV-irradiation was selected to induce photopolymerisation due to its many advantages including fast polymerization rate at low temperature, and ease of hydrogel shaping.³² Irgacure 2959 has been demonstrated to cause minimal toxicity to a wide range of mammalian cells,³³ and was employed as a photoinitiator in this study. Further lyophilisation of the hydrogel produced highly porous structures (Fig. 1d Step 4). HPC-MA-10%, HPC-MA-15% and HPC-MA-20% hydrogel samples were prepared and subjected to characterization, and will be described in later sections.

Swelling ratio and mechanical properties

Fig. 2 summarizes the swelling ratios (SRs) of the lyophilised HPC scaffolds in water and the storage modulus of hydrated HPC-MA at room temperature. The swelling ratio is a measure of wettability of a material. Hydrogels with high swelling ratio are highly permeable, which facilitates oxygen, nutrient and metabolites exchange, and are considered as promising materials for tissue scaffolding.³⁴ It was seen that the three different HPC-MA concentrations exhibit high SR attributed to the presence of hydroxyl groups on the HPC chain that attract water molecules from the surrounding environment. The SR was found to be decreasing with increasing HPC-MA concentration ($p < 0.05$, $n = 4$), whereas HPC-MA-10% had the highest SR of 35.83 while the SRs of HPC-MA-15% and HPC-MA-20% were found to be 19.16 and 12.94, respectively. It is well known that the crosslinking density has a strong influence on the swelling ratio of the hydrogel.^{35–39} The number of crosslinking bonds per volume, known as the crosslinking density, increases with increasing polymer concentration. As the crosslinking density

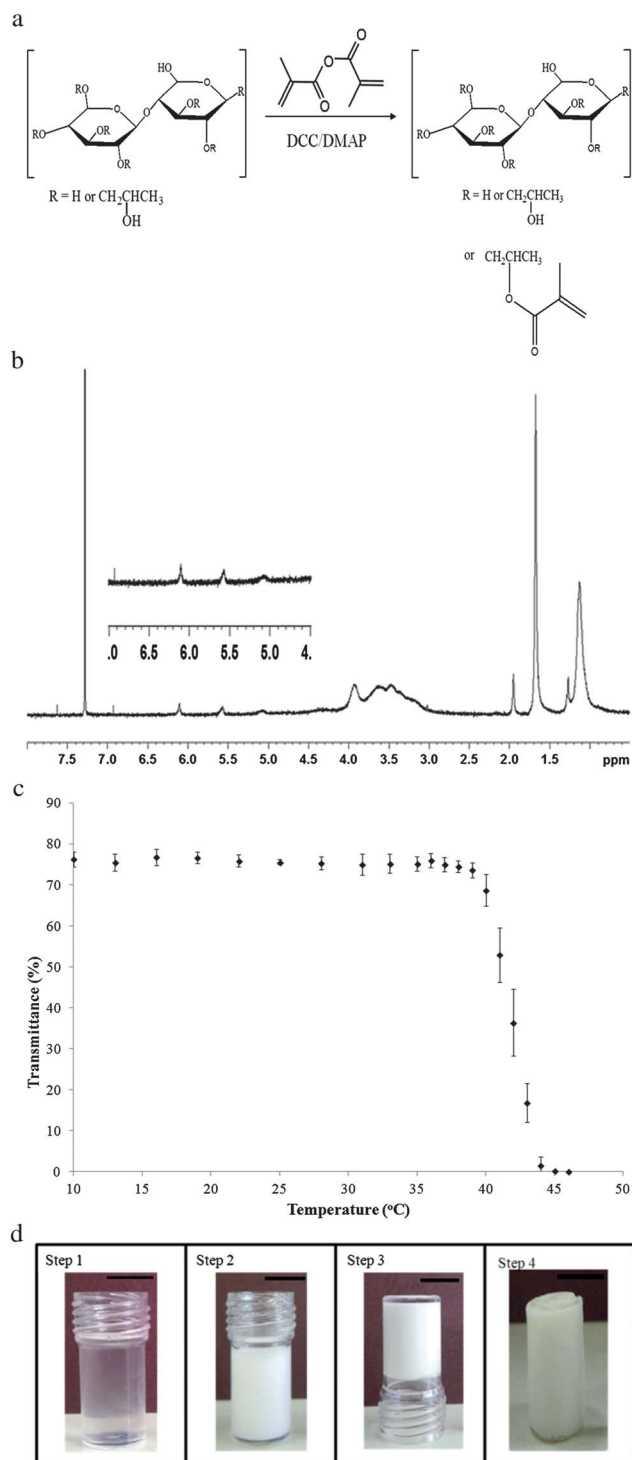


Fig. 1 (a) Synthesis scheme of HPC-MA. (b) NMR of HPC-MA in CDCl_3 . (c) Turbidimetry measurement for HPC-MA-10 wt%. The data are shown as mean values with standard deviation as error bars in the form of mean value \pm standard deviation. (d) Preparation of the HPC-MA scaffold (scale bar 1.0 cm) from (Step 1) a homogenous solution of HPC-MA-10 wt% at room temperature, to (Step 2) phase separated colloidal fluid at ~ 45 $^\circ\text{C}$, (Step 3) crosslinked heterogeneous gel at room temperature and (Step 4) freeze-dried scaffold.

increases, the water molecules and water-soluble substances will find it hard to infiltrate into a densely crosslinked network, thus, resulting in a lower swelling ratio.

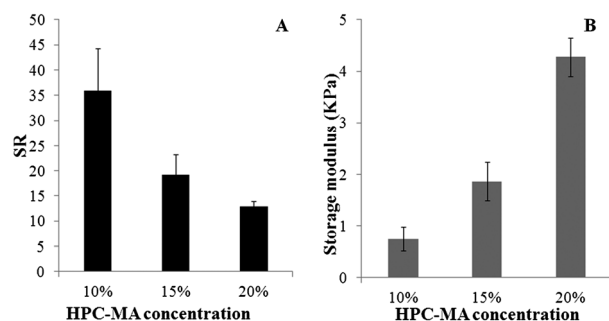


Fig. 2 Swelling ratio (A) and storage modulus (kPa) (B) of HPC-MA-10 wt%, 15 wt% and 20 wt% hydrogels at room temperature respectively. The data are shown as mean values with standard deviation as error bars in the form of mean value \pm standard deviation.

Biological tissues and organs are soft viscoelastic materials, which display a wide range of mechanical properties tailored for their specific physiological function. The change in tissue stiffness is generally associated with pathological disease or tissue dysfunction.^{10,40} Accumulative evidence suggests that substrate mechanics and the topography of extracellular microenvironment can regulate cell phenotype similar to the influence of biochemical signals.^{41,42} Mechanical strength is therefore an important property of hydrogel scaffolds. For tissue regeneration to be successful, it is believed that the mechanical properties of the scaffold should match roughly the mechanical properties of tissue growth in order to provide cells with instructive microenvironment. The storage modulus of HPC-MA-10%, 15% and 20% was found to be 0.75, 1.87 and 4.28 kPa, respectively. As expected, the storage modulus increased with increasing HPC-MA concentration ($p < 0.05$, $n = 4$). It is well known that the hydrogel with higher precursor mass exhibits stronger mechanical properties, as the crosslinking degree increases due to the formation of a longer attached chain.^{36,43} The storage moduli of the HPC-MA hydrogels are comparable to those of soft tissues and organs such as brain, lymph node, mammary gland, liver, breast tumor and kidney,¹⁰ and suggest that the HPC-MA hydrogels can be used as tissue scaffolds to mimic these soft tissues. These results prove that the swelling ratio and mechanical properties of the hydrogel can be tuned by altering the crosslinking density.³⁶

Physiochemical properties of hydrogels

The HPC-MA scaffold with interconnected porous structure was fabricated by polymerizing colloidal HPC-MA solution followed by lyophilisation. It is well known that polymerization in colloidal solution generates an open-cell structure *i.e.* an interconnected porous structure with water channels throughout the network.^{43,44} Fig. 3A–F show the cross-sections of the three different concentrations of lyophilised HPC-MA scaffolds visualized and characterized using SEM at low and high magnifications. As expected, the SEM images revealed that all the HPC-MA scaffolds were highly porous with interconnected pores. The degree of interconnection was assessed by mercury porosimetry and focused ion beam milling-scanning

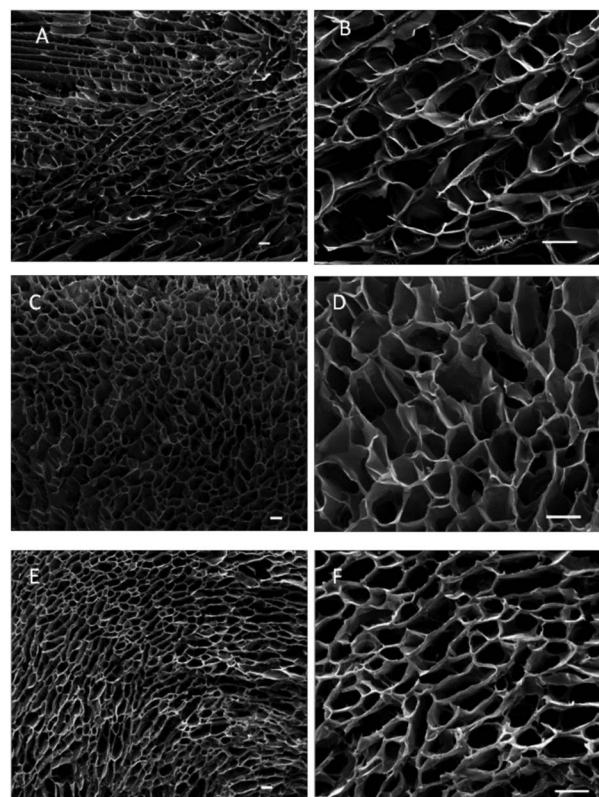


Fig. 3 Pore size and morphology of HPC-MA scaffolds. (A and B), (C and D), (E and F) are representative cross-sectional SEM micrographs of lyophilised HPC-MA-10 wt%, 15 wt% and 20 wt%, at low and high magnifications (scale bar 100 μ m), respectively.

electron microscopy (FIB-SEM). The mercury porosimeter method is a common technique used by many groups to quantify interconnected porosity, as mercury porosimetry only measures the interconnected channels in a microstructure, the result has therefore been used to verify the interconnectivity of a microstructure.^{45–49} FIB milling has been used as a new technique to assess the 3D porosity of the hydrogel,²⁹ the FIB/SEM also allows a precise visualization of the interconnectivity of the scaffold.

Representative images in Fig. 4a(A) and (B) showed the cross-section of HPC-MA-10% before FIB milling and after a 50 μ m layer has been removed, respectively. Interconnections between different pores in these two layers were observed, which further verified the interconnectivity of the scaffolds. Such interconnected pores are needed for cell infiltration, unrestricted cell–cell signalling, and nutrient transport to take place. Mercury porosimeter measurements further confirmed the presence of highly interconnected macroporous structures in HPC-MA-10%, 15 wt% and 20 wt%. Representative pore size distribution graphs are shown in Fig. 4b. All scaffolds had pore size ranging from 30 to 330 μ m. HPC-MA-10%, HPC-MA-15% and HPC-MA-20% exhibited a median pore diameter of 69.4, 45.1, and 42.4 μ m, respectively. The pore size of the HPC-MA scaffold depends on the polymer concentration as expected. It was found that a decrease in the average value of median pore size ($p < 0.05$, $n = 4$) was associated with an increase in the polymer concentration as

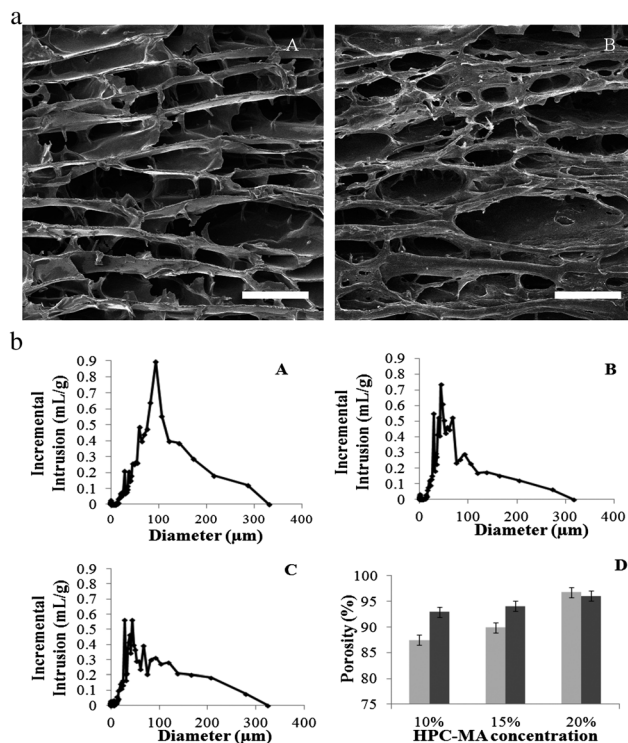


Fig. 4 (a) FIB/SEM of HPC-MA-10 wt% (scale bar 100 μm), top view SEM image of the scaffold before milling (A), after a layer of approximately 50 μm in thickness milled off by FIB (B). (b) Pore size distribution of HPC-MA-10 wt% (A), 15 wt% (B) and 20 wt% (C); porosity (■) and interconnected porosity (■) of the HPC-MA scaffold (D). The data are shown as mean values with standard deviation as error bars in the form of mean value ± standard deviation.

expected. It is well known that the high crosslinking density will result in a smaller pore size due to the highly intramolecularly crosslinked copolymers.⁵⁰ Nonetheless, all three scaffolds were highly porous. The interconnected porosities determined by mercury intrusion porosimetry for HPC-MA-10%, HPC-MA-15%, and HPC-MA-20% were found to be $93 \pm 0.8\%$, $94 \pm 0.7\%$, and $96 \pm 0.9\%$, respectively. There is no significant difference between the porosity measurements obtained using the solvent replacement method and the porosity measurements obtained using mercury intrusion porosimetry ($p > 0.05$, $n = 4$). These results suggest that an induced phase separation technique is able to create a highly interconnected macroporous and high porosity 3D structure.

Degradation profile

For successful tissue regeneration, a tissue scaffold should provide sufficient mechanical support for cell proliferation before new tissue growth, but it should degrade and resorb at a rate that matches the new tissues growth rate.⁵¹ Cellulose possesses many favourable properties that make it attractive as a tissue scaffold material.²⁶ However, cellulose is generally regarded to have limited *in vivo* degradability due to the absence of appropriate hydrolases. The subcutaneous implantation of cellulose sponge was studied⁵² and a decrease in implant size was observed after 16 weeks, however it is suggested that the complete disappearance of cellulose sponge will take longer

than 60 weeks. The degradation of an allyl isocyanate modified HPC hydrogel was studied²⁶ over a period of 12 weeks and observed no significant degradation. To improve the degradability of the HPC hydrogel, a bifunctional linker MA was incorporated into HPC as a pendant group. It is well known that MA can be radically polymerized to form a polyester network and the resulting ester linkages are hydrolytically degradable.^{53,54} The hydrolytic degradation of HPC-MA hydrogels was monitored by measuring the weight loss of samples over time, and the results were presented in terms of weight percentage remaining against time. Fig. 5 shows the degradation profile of HPC-MA hydrogels with different polymer concentrations over a period of 40 days in PBS. All HPC-MA hydrogels underwent degradation after 5 days of incubation in PBS, indicating that the use of degradable crosslinker methacrylate anhydride has greatly improved the degradability of the cellulose hydrogel. The degradation of HPC-MA-10% was the fastest with a remaining weight of approximately 10% after 40 days. The percentage of the remaining weight of HPC-MA-15% was approximately 30% after 40 days, whereas the percentage of the remaining weight of HPC-MA-20% was approximately 50% after 40 days. As expected, the hydrogels prepared from higher HPC-MA concentration showed slower degradation ($p < 0.05$, $n = 5$). It is known that polyesters degrade by hydrolytic cleavage of the ester linkage, the degradation rate is highly dependent on the crosslinking density.^{55,56} The degradation is slower in the tightly crosslinked network due to the lower water accessibility, hence slower hydrolysis rate. The data obtained in this work illustrate that varying the polymer concentration can alter the degradation rate of the HPC-MA hydrogel.

Surface functionalization of the scaffold and cell proliferation in the hydrogel scaffold

Most mammalian cells are anchorage dependent, therefore, cell adhesion to the extracellular matrix (ECM) plays an important role in regulating cell survival, cell cycle progression, tissue-specific phenotype expression, organogenesis, wound healing, tissue homeostasis and remodelling.⁵⁷ An ideal tissue scaffold

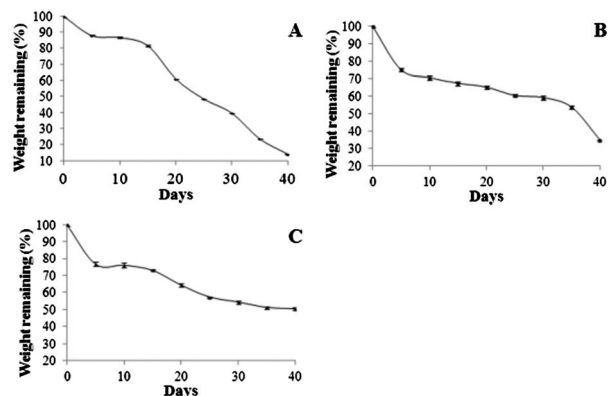


Fig. 5 Degradation profile of HPC-MA-10 wt% (A), 15 wt% (B) and 20 wt% (C). The data are shown as mean values with standard deviation as error bars in the form of mean value ± standard deviation, and the standard deviations appear to be small.

should provide cell adhesion sites. HPC as a commercial derivative of cellulose has many favourable properties as biomaterials,^{23,58} but it does not contain any cell-recognizable signal molecules that can mediate mammalian cell adhesion. To achieve cell-substrate interaction, the scaffold surface can be functionalized with biochemical cues after scaffold fabrication.⁵⁹ To demonstrate the feasibility to introduce biochemical cues to the HPC-MA hydrogel to enable cell adhesion, the surface of HPC-MA-10% was activated by CDI followed by conjugation with gelatin. Gelatin contains arginine-glycine-aspartate (RGD) peptide sequence that can mediate cell-substrate interaction.^{34,60} To evaluate the feasibility of using HPC-MA hydrogels as 3D scaffolds for adipose tissue engineering, ASCs were cultured for 21 days in the scaffold with adipogenic medium and analyzed using SEM. Fig. 6A and B show the presence of ASCs on the surface and cross-section of scaffolds, respectively. These results indicated that the HPC-MA scaffold supported the growth of ASCs, as well as infiltration into the scaffold (Fig. 6B), demonstrating its high-interconnected porosity. In addition, using alamarBlue® as an indirect indicator of cell proliferation, the number of ASCs was observed to increase gradually over a period of 7 days from the cell proliferation data, which indicated that the material properties of the scaffold supported the growth of ASCs (Fig. 7). It is noted that cells are seeded onto HPC-MA scaffolds using a typical static seeding method which may not result in optimal seeding efficiency or optimal cell distribution. In a subsequent study, an alternative cell seeding method such as the surface acoustic wave driven seeding method⁶¹ can be employed to improve the seeding efficiency.

Adipogenic characterization

The differentiation capability of ASCs that were cultured in the scaffolds with adipogenic supplements was also studied. It is very well known that adipogenesis is enhanced on scaffolds with stiffness similar to that of *in vivo* adipose tissue.^{62,63} After studying the mechanical characterization results described

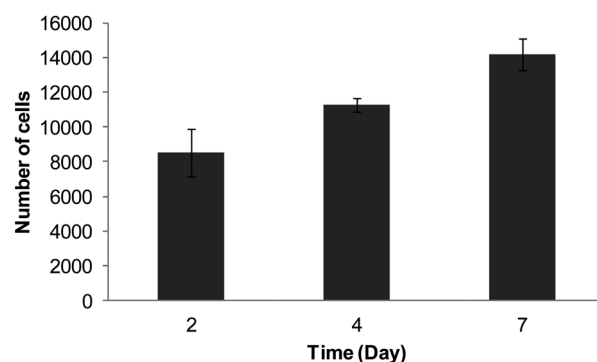


Fig. 7 Number of ASCs in the HPC-MA-10 wt% scaffolds over a period of one week.

above, HPC-MA-10% was selected for this study since it exhibits a storage modulus closest to that of adipose tissue⁶⁴ in comparison to the other two scaffold formulations. Adipogenic differentiation of ASCs into adipocytes inside the scaffolds was evaluated by Oil Red O (ORO) staining.⁶⁵ Fig. 8A illustrates the typical ORO staining image of a fat tissue, while Fig. 8B and C show the oil content of Day 14 ASCs grown on a two-dimensional (2D) tissue culture plate (TCP) without and with adipogenic medium, respectively. It was observed that ASCs did not differentiate into adipocytes in the absence of adipogenic medium. From Fig. 8C, an increase in the oil content in the ASCs grown in the scaffolds could be observed over a period of 14 days. From the results, an absence of stained lipid content was observed on Day 2, thereby showing the absence of adipogenesis at this initial stage. From Day 4 onwards, lipid droplets that were stained red were observed and the amount of lipid content increases with longer period of culture. A large amount of oil content was observed on Day 14. Adipogenic differentiation of ASCs into adipocytes in the scaffolds was further confirmed by the release of adiponectin and leptin into the medium. Similar to ORO staining, both adiponectin (Fig. 9A)

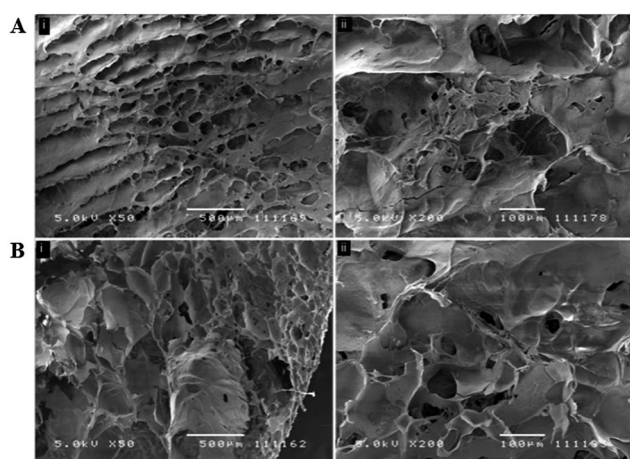


Fig. 6 SEM micrographs illustrating the presence of ASCs on the (A) surface and (B) cross-section of Day 14 cell cultured HPC-MA-10 wt% scaffolds at (i) 50 \times and (ii) 200 \times magnifications.

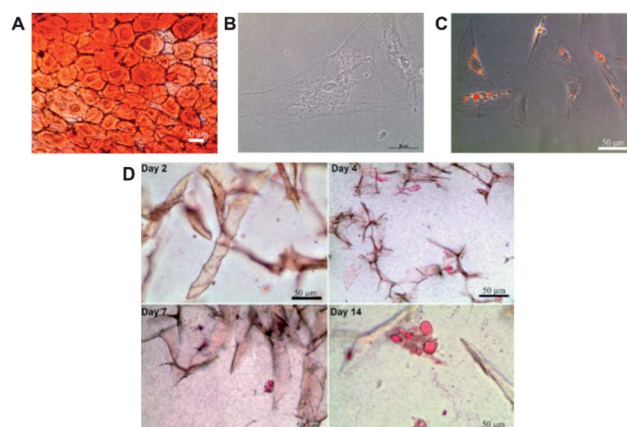


Fig. 8 Oil Red O staining of the lipid droplets of (A) fat tissue, (B) ASCs grown on a 2D TCP without adipogenic supplement, (C) ASCs grown on a 2D TCP with adipogenic supplement (Day 14), and (D) ASCs grown in the 3D HPC-MA-10 wt% scaffold over a period of 14 days and lipid droplets were observed to be present from Day 4 onwards. Scale bar 50 μ m.

and leptin (Fig. 9B) release began on Day 4, and the amount of adiponectin and leptin released increased significantly after 14 days of culture ($p < 0.05$, $n = 3$). In addition, the amount of adiponectin released was much higher than leptin over the same period of time. Hence, ASCs were also capable of differentiating into adipocytes in the scaffolds. Evidence is emerging that physical culture conditions play a major role in determining stem cell fate to an extent that surpasses the influence of growth and differentiation factors.^{66–68} Of particular relevance to this work is the discovery that geometric factors play an important role in regulating the commitment of stem cell fate. For instance, well-spread mesenchymal stem cells (MSCs) underwent osteogenesis, while un-spread cells underwent adipogenesis.^{69,70} Ruiz and Chen demonstrated that MSCs underwent osteogenesis at convex edges and adipogenesis at concave edges.⁷¹ It was observed that the HPC-MA scaffolds contain a large number of concave pores compared to convex edges, the provision of a large number of concave pores in HPC-MA scaffolds may also promote adipogenesis of ASCs.

Gene expression (RT-PCR)

Adipogenic differentiation of ASCs in the scaffolds was further confirmed by evaluating the gene expression levels of adipogenic markers. The fold change values for ASCs cultured with adipogenic supplements in the scaffold were compared to the undifferentiated ASCs cultured on a TCP (control) for the adipogenic genes (PPARG, LPL, leptin and adiponectin). ASCs subjected to differentiation in the scaffold displayed fold change values that were much higher than the control for early adipogenic markers (PPARG and LPL) ($p < 0.05$, $n = 3$) (Fig. 10A) and late adipogenic markers (adiponectin and leptin) ($p < 0.05$, $n = 3$) (Fig. 10B). The upregulation of adipogenic stem cell markers suggests that the 3D scaffold together with the adipogenic supplements led to the differentiation of ASCs into adipocytes. The successful adipogenesis could also be attributed to the use of a 3D matrix with mechanical stiffness matching that of native adipose tissue. It is worthwhile to mention that scaffold mechanical properties play an important role in directing stem cell niche and ASCs are capable of

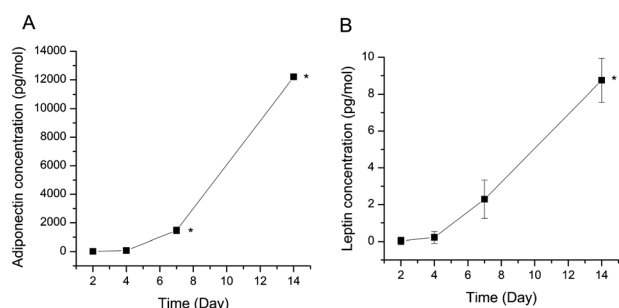


Fig. 9 Amount of (A) adiponectin and (B) leptin released into the medium over a period of 14 days. Both adiponectin and leptin were released from Day 4 onwards, and the amount released increased significantly after 14 days of culture ($*p < 0.05$, $n = 3$). The data are shown as mean values with standard deviation as error bars in the form of mean value \pm standard deviation, and the standard deviations appear to be small.

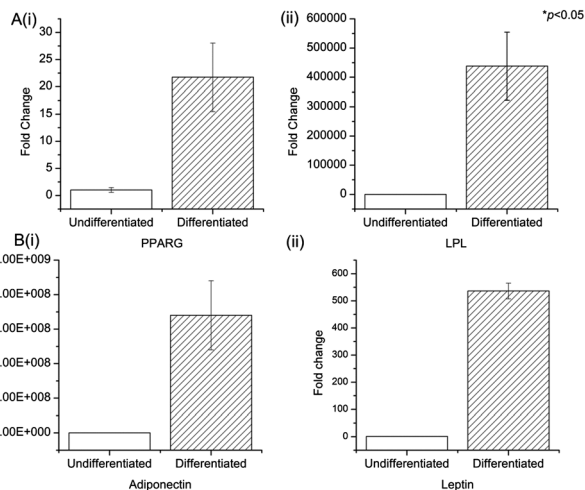


Fig. 10 PCR results for ASCs cultured in the scaffolds with adipogenic supplements compared to undifferentiated ASCs cultured on a TCP (control). Fold change values of the samples were shown for (A) early adipogenic markers (i) PPARG and (ii) LPL, and (B) late adipogenic markers (i) adiponectin and (ii) leptin. The upregulation of adipogenic markers suggests that the 3D microenvironment together with the adipogenic supplements led to the differentiation of ASCs into adipocytes ($*p < 0.05$, $n = 3$).

differentiating into a variety of cell types not limiting to adipocyte.^{9,13,14} In a subsequent study, HPC-MA scaffolds with higher storage modulus can be employed as a 3D adipose stem cells culture system. The effect of increasing storage modulus of the scaffold on adipose stem cell fate is currently under investigation.

Conclusions

In this study, a novel class of 3D macroporous hydroxypropyl cellulosic scaffolds were developed by UV polymerizing MA conjugated HPC at its biphasic phase. The scaffolds exhibited high swelling ratio, biodegradability, cytocompatibility, and mechanical integrity similar to those of soft tissue in particular adipose tissue. The pore structure of HPC-MA scaffolds was highly interconnected as a result of the use of the phase separation technique followed by lyophilisation. By applying the same principle, macroporous scaffolds can be prepared using other responsive polymers that can form colloidal systems induced by environmental stimuli such as temperature and pH change. The HPC-MA scaffolds promoted ASC infiltration, proliferation and adipogenesis. Hence, these interconnected macroporous hydrogels are promising 3D *in vitro* adipocyte culture systems that can be used for studying tissue-inherent interactions such as 3D cell–matrix interactions.

Acknowledgements

This work was funded by Australia Research Council (ARC) Discovery Project Grants DP120102570 and Singapore Ministry of Education AcRF Tier 2 ARC16/11. This work was performed in part at the Melbourne Centre for Nanofabrication, an initiative funded jointly by the Commonwealth of Australia and the

Victorian government. The authors acknowledge the facilities, and the scientific and technical assistance, of the Australian Microscopy & Microanalysis Research Facility at the RMIT Microscopy & Microanalysis Facility, at RMIT University.

Notes and references

- 1 P. Bauer-Kreisel, A. Goepferich and T. Blunk, *Adv. Drug Delivery Rev.*, 2010, **62**, 798–813.
- 2 M. L. Moya, M. H. Cheng, J. J. Huang, M. E. Francis-Sedlak, S. W. Kao, E. C. Opara and E. M. Brey, *Biomaterials*, 2010, **31**, 2816–2826.
- 3 E. Thian, J. Huang, M. Vickers, S. Best, Z. Barber and W. Bonfield, *J. Mater. Sci.*, 2006, **41**, 709–717.
- 4 S. Q. Liu, R. Tay, M. Khan, P. L. Rachel Ee, J. L. Hedrick and Y. Y. Yang, *Soft Matter*, 2010, **6**, 67–81.
- 5 C. T. Gomillion and K. J. L. Burg, in *Comprehensive Biomaterials*, ed. D. Paul, Elsevier, Oxford, 2011, pp. 529–539.
- 6 E. Sachlos and J. T. Czernuszka, *Eur. Cells Mater.*, 2003, **5**, 29–39, discussion 39–40.
- 7 T. B. Woodfield, J. Malda, J. de Wijn, F. Peters, J. Riesle and C. A. van Blitterswijk, *Biomaterials*, 2004, **25**, 4149–4161.
- 8 R. A. Marklein and J. A. Burdick, *Adv. Mater.*, 2010, **22**, 175–189.
- 9 L. E. Flynn, *Biomaterials*, 2010, **31**, 4715–4724.
- 10 I. Levental, P. C. Georges and P. A. Janmey, *Soft Matter*, 2007, **3**, 299–306.
- 11 J. M. Gimble, A. J. Katz and B. A. Bunnell, *Circ. Res.*, 2007, **100**, 1249–1260.
- 12 B. Lindroos, R. Suuronen and S. Miettinen, *Stem Cell Rev.*, 2011, **7**, 269–291.
- 13 H. Mizuno, *J. Nippon Med. Sch.*, 2009, **76**, 56–66.
- 14 P. A. Zuk, M. Zhu, P. Ashjian, D. A. De Ugarte, J. I. Huang, H. Mizuno, Z. C. Alfonso, J. K. Fraser, P. Benhaim and M. H. Hedrick, *Mol. Biol. Cell*, 2002, **13**, 4279–4295.
- 15 B. Galateanu, S. Dinescu, A. Cimpean, A. Dinischiotu and M. Costache, *Int. J. Mol. Sci.*, 2012, **13**, 15881–15900.
- 16 L. Girandon, N. Kregar-Velikonja, K. Bozikov and A. Barlic, *Folia Biol.*, 2011, **57**, 47–56.
- 17 L. Flynn and K. A. Woodhouse, *Organogenesis*, 2008, **4**, 228–235.
- 18 F. J. O'Brien, B. A. Harley, I. V. Yannas and L. J. Gibson, *Biomaterials*, 2005, **26**, 433–441.
- 19 S. H. Oh, I. K. Park, J. M. Kim and J. H. Lee, *Biomaterials*, 2007, **28**, 1664–1671.
- 20 M. Sabir, X. Xu and L. Li, *J. Mater. Sci.*, 2009, **44**, 5713–5724.
- 21 B. Subia, J. Kundu and S. C. Kundu, *Tissue Eng.*, 2010, **524**.
- 22 Y. Ikada, *Tissue Engineering: Fundamentals and Applications, Interface Science and Technology*, Elsevier, 2006.
- 23 J. L. Drury and D. J. Mooney, *Biomaterials*, 2003, **24**, 4337–4351.
- 24 Q. Cai, J. Yang, J. Bei and S. Wang, *Biomaterials*, 2002, **23**, 4483–4492.
- 25 N. Soykeabkaew, C. Sian, S. Gea, T. Nishino and T. Peijs, *Cellulose*, 2009, **16**, 435–444.
- 26 Z. Yue, F. Wen, S. Gao, M. Y. Ang, P. K. Pallathadka, L. Liu and H. Yu, *Biomaterials*, 2010, **31**, 8141–8152.
- 27 M. A. Hussain, *J. Polym. Sci., Part A: Polym. Chem.*, 2008, **46**, 747–752.
- 28 J. M. Pachence, M. P. Bohrer and J. Kohn, in *Principles of Tissue Engineering*, ed. L. Robert, L. Robert and V. Joseph, Academic Press, Burlington, 3rd edn, 2007, pp. 323–339.
- 29 A. Al-Abboodi, J. Fu, P. M. Doran and P. P. Y. Chan, *Biotechnol. Bioeng.*, 2013, **110**, 318–326.
- 30 W. Dong, H. Li, M. Chen, Z. Ni, J. Zhao, H. Yang and P. Gijssman, *J. Polym. Res.*, 2011, **18**, 1239–1247.
- 31 G. D. Nicodemus and S. J. Bryant, *Tissue Eng., Part B*, 2008, **14**, 149–165.
- 32 R. S. Benson, *Nucl. Instrum. Methods Phys. Res., Sect. B*, 2002, **191**, 752–757.
- 33 C. G. Williams, A. N. Malik, T. K. Kim, P. N. Manson and J. H. Elisseeff, *Biomaterials*, 2005, **26**, 1211–1218.
- 34 L.-S. Wang, J. E. Chung, P. Pui-Yik Chan and M. Kurisawa, *Biomaterials*, 2010, **31**, 1148–1157.
- 35 M. Davidovich-Pinhas and H. Bianco-Peled, *Carbohydr. Polym.*, 2010, **79**, 1020–1027.
- 36 F. Lee, J. E. Chung and M. Kurisawa, *J. Controlled Release*, 2009, **134**, 186–193.
- 37 W.-F. Lee and W.-H. Chiang, *J. Appl. Polym. Sci.*, 2004, **91**, 2135–2142.
- 38 D. Singh, D. Kuckling, V. Koul, V. Choudhary, H.-J. Adler and A. K. Dinda, *Eur. Polym. J.*, 2008, **44**, 2962–2970.
- 39 D. Wang, D. J. T. Hill, F. Rasoul and A. K. Whittaker, *Radiat. Phys. Chem.*, 2011, **80**, 207–212.
- 40 W. L. K. Chen and C. A. Simmons, *Adv. Drug Delivery Rev.*, 2011, **63**, 269–276.
- 41 G. C. Reilly and A. J. Engler, *J. Biomech.*, 2010, **43**, 55–62.
- 42 L.-S. Wang, J. Boulaire, P. P. Y. Chan, J. E. Chung and M. Kurisawa, *Biomaterials*, 2010, **31**, 8608–8616.
- 43 L. S. Wang, P. Y. Chow, T. T. Phan, I. J. Lim and Y. Y. Yang, *Adv. Funct. Mater.*, 2006, **16**, 1171–1178.
- 44 B. G. Kabra, S. H. Gehrke and R. J. Spontak, *Macromolecules*, 1998, **31**, 2166–2173.
- 45 V. Karageorgiou and D. Kaplan, *Biomaterials*, 2005, **26**, 5474–5491.
- 46 J. Ma, C. Wang and K. W. Peng, *Biomaterials*, 2003, **24**, 3505–3510.
- 47 R. M. Pilliar, M. J. Filiaggi, J. D. Wells, M. D. Grynepas and R. A. Kandel, *Biomaterials*, 2001, **22**, 963–972.
- 48 E. Romero and P. Simms, *Geotech. Geol. Eng.*, 2008, **26**, 705–727.
- 49 Ž. Zuzana, G. Eva and P. Willi, *Process. Appl. Ceram.*, 2008, **2**, 1–8.
- 50 Q. Liu, Y. Li, S. Shen and Z. Shanshan, *Mater. Chem. Phys.*, 2011, **125**, 315–318.
- 51 R. van Dijkhuizen-Radersma, L. Moroni, A. v. Apeldoorn, Z. Zhang and D. Grijpma, in *Tissue Engineering*, ed. B. Clemens van, T. Peter, L. Anders, H. Jeffrey, F. W. David, C. Ranieri, D. d. B. Joost and S. Jérôme, Academic Press, Burlington, 2008, pp. 193–221.
- 52 M. Mårtson, J. Viljanto, T. Hurme, P. Laippala and P. Saukko, *Biomaterials*, 1999, **20**, 1989–1995.
- 53 K. S. Anseth, V. R. Shastri and R. Langer, *Nat. Biotechnol.*, 1999, **17**, 156–159.

- 54 L. S. Nair and C. T. Laurencin, *Prog. Polym. Sci.*, 2007, **32**, 762–798.
- 55 C. B. Hutson, J. W. Nichol, H. Aubin, H. Bae, S. Yamanlar, S. Al-Haque, S. T. Koshy and A. Khademhosseini, *Tissue Eng., Part A*, 2011, **17**, 1713–1723.
- 56 Q. Li, J. Wang, S. Shahani, D. D. N. Sun, B. Sharma, J. H. Elisseeff and K. W. Leong, *Biomaterials*, 2006, **27**, 1027–1034.
- 57 A. J. García and D. Boettiger, *Biomaterials*, 1999, **20**, 2427–2433.
- 58 C. Chang and L. Zhang, *Carbohydr. Polym.*, 2011, **84**, 40–53.
- 59 Y. Ke, Y. J. Wang, L. Ren, Q. C. Zhao and W. Huang, *Acta Biomater.*, 2010, **6**, 1329–1336.
- 60 Y. Chen and L. Liu, *Adv. Drug Delivery Rev.*, 2012, **64**, 640–665.
- 61 H. Li, J. R. Friend and L. Y. Yeo, *Biomaterials*, 2007, **28**, 4098–4104.
- 62 A. G. Cristancho and M. A. Lazar, *Nat. Rev. Mol. Cell Biol.*, 2011, **12**, 722–734.
- 63 C. Yu, J. Bianco, C. Brown, L. Fuetterer, J. F. Watkins, A. Samani and L. E. Flynn, *Biomaterials*, 2013, **34**, 3290–3302.
- 64 K. Comley and N. A. Fleck, *Int. J. Solids Struct.*, 2010, **47**, 2982–2990.
- 65 D. H. Stacey, S. E. Hanson, G. Lahvis, K. A. Gutowski and K. S. Masters, *Tissue Eng., Part A*, 2009, **15**, 3389–3399.
- 66 F. Guilak, D. M. Cohen, B. T. Estes, J. M. Gimble, W. Liedtke and C. S. Chen, *Cell Stem Cell*, 2009, **5**, 17–26.
- 67 N. Huebsch, P. R. Arany, A. S. Mao, D. Shvartsman, O. A. Ali, S. A. Bencherif, J. Rivera-Feliciano and D. J. Mooney, *Nat. Mater.*, 2010, **9**, 518–526.
- 68 M. P. Lutolf, P. M. Gilbert and H. M. Blau, *Nature*, 2009, **462**, 433–441.
- 69 K. A. Kilian, B. Bugarija, B. T. Lahn and M. Mrksich, *Proc. Natl. Acad. Sci. U. S. A.*, 2010, **107**, 4872–4877.
- 70 R. McBeath, D. M. Pirone, C. M. Nelson, K. Bhadriraju and C. S. Chen, *Dev. Cell*, 2004, **6**, 483–495.
- 71 S. A. Ruiz and C. S. Chen, *Stem Cells*, 2008, **26**, 2921–2927.